EPJ manuscript No.
(will be inserted by the editor)

arXiv:1010.1675v3 [nucl-ex] 10 Feb 2011

Hyperon production in Ar+KCl collisions at 1.76A GeV

G. Agakishiev[6], A. Balanda[3,†], B. Bannier[5], R. Bassini[9], D. Belver[16], A. Belyaev[6], A. Blanco[2], M. Böhmer[12], J. L. Boyard[14], P. Cabanelas[16], E. Castro[16], S. Chernenko[6], T. Christ[12], M. Destefanis[8], J. Díaz[17], F. Dohrmann[5], A. Dybczak[3], T. Eberl[12], E. Epple[11], L. Fabbietti[11], O. Fateev[6], P. Finocchiaro[1], P. Fonte[2,A], J. Friese[12], I. Fröhlich[7], T. Galatyuk[7], J. A. Garzón[16], R. Gernhäuser[12], A. Gil[17], C. Gilardi[8], M. Golubeva[10], D. González-Díaz[4], F. Guber[10], M. Gumberidze[14], M. Heilmann[7], T. Heinz[4], T. Hennino[14], R. Holzmann[4], P. Huck[12], I. Iori[9,C,†], A. Ivashkin[10], M. Jurkovic[12], B. Kämpfer[5,B], K. Kanaki[5], T. Karavicheva[10], D. Kirschner[8], I. Koenig[4], W. Koenig[4], B. W. Kolb[4], R. Kotte[5], F. Krizek[15], R. Krücken[12], W. Kühn[8], A. Kugler[15], A. Kurepin[10], S. Lang[4], J. S. Lange[8], K. Lapidus[11,E], T. Liu[14], L. Lopes[2], M. Lorenz[7,*], L. Maier[12], A. Mangiarotti[2], J. Markert[7], V. Metag[8], B. Michalska[3], J. Michel[7], D. Mishra[8], E. Morinière[14], J. Mousa[13], C. Müntz[7], L. Naumann[5], J. Otwinowski[3], Y. C. Pachmayer[7], M. Palka[7], Y. Parpottas[13], V. Pechenov[4], O. Pechenova[7], T. Pérez Cavalcanti[8], J. Pietraszko[7], W. Przygoda[3], B. Ramstein[14], A. Reshetin[10], M. Roy-Stephan[14], A. Rustamov[4], A. Sadovsky[10], B. Sailer[12], P. Salabura[3], A. Schmah[4,F,*], E. Schwab[4], J. Siebenson[11], Yu.G. Sobolev[15], S. Spataro[8,D], B. Spruck[8], H. Ströbele[7], J. Stroth[7,4], C. Sturm[4], A. Tarantola[7], K. Teilab[7], P. Tlusty[15], M. Traxler[4], R. Trebacz[3], H. Tsertos[13], V. Wagner[15], M. Weber[12], C. Wendisch[5], M. Wisniowski[3], T. Wojcik[3], J. Wüstenfeld[5], S. Yurevich[4], Y. Zanevsky[6], P. Zhou[5], P. Zumbruch[4]

(HADES collaboration)
[1]Istituto Nazionale di Fisica Nucleare - Laboratori Nazionali del Sud, 95125 Catania, Italy
[2]LIP-Laboratório de Instrumentação e Física Experimental de Partículas , 3004-516 Coimbra, Portugal
[3]Smoluchowski Institute of Physics, Jagiellonian University of Cracow, 30-059 Kraków, Poland
[4]GSI Helmholtzzentrum für Schwerionenforschung GmbH, 64291 Darmstadt, Germany
[5]Institut für Strahlenphysik, Forschungszentrum Dresden-Rossendorf, 01314 Dresden, Germany
[6]Joint Institute of Nuclear Research, 141980 Dubna, Russia
[7]Institut für Kernphysik, Goethe-Universität, 60438 Frankfurt, Germany
[8]II.Physikalisches Institut, Justus Liebig Universität Giessen, 35392 Giessen, Germany
[9]Istituto Nazionale di Fisica Nucleare, Sezione di Milano, 20133 Milano, Italy
[10]Institute for Nuclear Research, Russian Academy of Science, 117312 Moscow, Russia
[11]Excellence Cluster 'Origin and Structure of the Universe' , 85478 Munich, Germany
[12]Physik Department E12, Technische Universität München, 85748 München, Germany
[13]Department of Physics, University of Cyprus, 1678 Nicosia, Cyprus
[14]Institut de Physique Nucléaire (UMR 8608), CNRS/IN2P3 - Université Paris Sud, F-91406 Orsay Cedex, France
[15]Nuclear Physics Institute, Academy of Sciences of Czech Republic, 25068 Rez, Czech Republic
[16]Departamento de Física de Partículas, Univ. de Santiago de Compostela, 15706 Santiago de Compostela, Spain
[17]Instituto de Física Corpuscular, Universidad de Valencia-CSIC, 46971 Valencia, Spain
[A] also at ISEC Coimbra, Coimbra, Portugal
[B] also at Technische Universität Dresden, 01062 Dresden, Germany
[C] also at Dipartimento di Fisica, Università di Milano, 20133 Milano, Italy
[D] also at Dipartimento di Fisica Generale, Universita' di Torino, 10125 Torino, Italy
[E] also at Joint Institute of Nuclear Research, 141980 Dubna, Russia
[F] also at Lawrence Berkeley National Lab, Berkeley California 94720, United States

[*] corresponding author: Lorenz@Physik.uni-frankfurt.de, aschmah@lbl.gov
[†] deceased

Received: 24.12.2010 / Revised version: date

Abstract. We present transverse momentum spectra, rapidity distribution and multiplicity of Λ-hyperons measured with the HADES spectrometer in the reaction Ar(1.76A GeV)+KCl. The yield of Ξ^- is calculated from our previously reported $\Xi^-/(\Lambda+\Sigma^0)$ ratio and compared to other strange particle multiplicities. Employing a strangeness balance equation the multiplicities of the yet unmeasured $\Sigma^{\pm}$ hyperons can be estimated. Finally a statistical hadronization model is used to fit the yields of π^-, K^+, K^0_s, K^-, ϕ, Λ and Ξ^-. The resulting chemical freeze-out temperature of $T = (76 \pm 2)$ MeV is compared to the measured slope parameters obtained from fits to the transverse mass distributions of the different particles.

PACS. 25.75.-q, 25.75.Dw

1 Introduction

Strange hadrons are particularly suitable probes of the high density phase of nuclear matter produced in few GeV heavy ion collisions. For instance, from systematic investigations of subthreshold K^+ production tight constraints could be put on the nuclear equation of state at matter densities of 2-3 ρ_0 [1,2,3,4]. Furthermore, kaon phase space distributions and flow patterns are considered to be sensitive to the in-medium kaon potential [5,6,7]. On the other hand, due to strangeness conservation in the strong interaction, kaon production is intimately linked to the concurrent production of hyperons. While strange particle production is well understood in elementary NN collisions, in heavy ion reactions multi-step processes involving mesons or baryon resonances open up many additional production channels, even below threshold. Thus, strangeness-exchange channels like $\pi\Lambda \to NK^-$ have been proposed to explain the observed K^- yields [8,9,10], just as feeding through the $\phi \to K^+K^-$ decay has been [11].

Various aspects of strangeness production at SIS (Schwerionen Synchrotron at GSI Darmstadt) energies have been investigated by the FOPI and KaoS experiments (for reviews see [12,13]). Evidently, any in-depth understanding of strangeness production and propagation in heavy ion reactions requires information on all particles with open or hidden strangeness. The HADES collaboration has done a complete measurement in the system Ar+KCl at a bombarding energy of 1.76A GeV. Results on K^0_s production have been published already in [14], on K^+, K^- and ϕ-meson production in [11] and on the first observation at such a low beam energy of the double-strange Ξ^- hyperon in [15]. To complete the picture, hyperon production remains to be addressed and this is the purpose of the present paper. We report here on the results obtained with the HADES detector on Λ production, from which, by application of strangeness conservation, we could estimate also the yield of the (not directly observed) Σ hyperons. Furthermore, we compare our set of particle yields to the result of a statistical hadronization model and discuss the implications. Note that the FOPI collaboration performed a similar analysis of strangeness production in the system Ni+Ni at 1.93A GeV [16].

In Section 2 of this paper we give first a brief overview of the HADES detector and relevant details of the Ar+KCl data taking and then proceed to describe the employed particle identification and Λ reconstruction procedures. In section 3 we present spectra and production yields of the Λ hyperons. In section 4 the Λ result is used to extract the yield of the double-strange Ξ^- from our previously published Ξ^-/Λ ratio [15]. With all experimental yields established, strangeness balance is applied to estimate the yield of the unobserved charged Σ hyperons. We compare all yields obtained in Ar+KCl with respect to a statistical hadronization model and confront the fitted chemical freeze-out temperature with the measured slope parameters obtained from transverse mass distributions. Finally we summarize our findings in section 5.

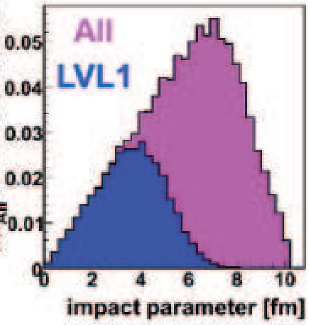

Fig. 1. Impact parameter distributions of all and LVL1 selected Ar+KCl reactions obtained from the UrQMD transport code [18].

2 Experimental setup

HADES is a charged-particle detector consisting of a 6-coil toroidal magnet centered on the beam axis and six identical detection sections located between the coils and covering polar angles between 18° and 85°. Each sector is equipped with a Ring-Imaging Cherenkov (RICH) detector followed by Multi-wire Drift Chambers (MDCs), two in front of and two behind the magnetic field, as well as a scintillator hodoscope (TOF/TOFino). Lepton identification is provided mostly by the RICH and supplemented at low polar angles with Pre-SHOWER chambers, mounted at the back of the apparatus. Hadron identification, however, is based on the time-of-flight and on the energy-loss information from TOF/TOFino, as well as from the MDC tracking chambers. A detailed description of HADES is given in [17].

An argon beam of $\sim 10^6$ particles/s was incident with a beam energy of 1.76A GeV on a four-fold segmented KCl target with a total thickness corresponding to 3.3 % interaction probability. A fast diamond start detector located upstream of the target was intercepting the beam and was used to determine the time-zero information. The data readout was started by a first-level trigger (LVL1) requiring a charged-particle multiplicity, $MUL \geq 16$, in the TOF/TOFino detectors. Based on a full GEANT simulation of the detector response to Ar+KCl events generated with the UrQMD transport model [18], we found that the event ensemble selected by this (LVL1) trigger condition has a mean number of participating nucleons ($\langle A_{part} \rangle$) equal to 38.5 ± 3.9. Figure 1 illustrates the impact parameter distributions obtained from UrQMD calculations for two event selections: all inelastic events and according to the experimental LVL1 trigger condition.

The particle identification was done by a velocity vs. momentum × polarity correlation, where the velocity was determined by the time-of-flight measurement in the TOF and TOFino scintillators with respect to the time-zero information and the tracked flight path. If needed, additional particle discrimination was gained from the energy-loss (dE/dx) information in the MDC and scintillators.

3 $\mathit{\Lambda}$ hyperon yield and spectra

3.1 $\mathit{\Lambda}$ identification

The particle identification of kaons, ϕ, π^- and $\mathit{\Xi}^-$ is described in [11,15,14]. Here we add only those details specific to the reconstruction of $\mathit{\Lambda}$ hyperons in their decay channel $\mathit{\Lambda} \rightarrow p + \pi^-$ (B.R. = 63.9%, $c\tau$=7.89 cm [19]). Note that at our beam energies the reconstructed $\mathit{\Lambda}$ yield contains also a contribution from decays of the slightly heavier $\mathit{\Sigma}^0$ baryon into a $\mathit{\Lambda}$ and a photon.

The decay products of the $\mathit{\Lambda}$ hyperons have been identified using the MDC dE/dx and time-of-flight information. The topology of the $\mathit{\Lambda}$ decay into p-π^- pairs has been used to suppress the combinatorial background of uncorrelated pairs. Cuts on the distance between the primary event vertex and the decay vertex (d_{V0}), on the distances between the proton (d_p), respectively the π^- (d_{π^-}) track and the primary vertex, on the distance of closest approach between the two tracks (d_{dca}) and on the distance of the reconstructed mother particle trajectory to the primary vertex ($d_{p\pi^-}$) were applied. Furthermore, a minimum opening angle ($\alpha_{p\pi^-}$) was required to guarantee a good decay vertex resolution. All selections used for the analysis are listed in Table 1. For an estimation of the systematic errors, the cut values have been varied within reasonable limits. In total, 28 different cut combinations were thus investigated, resulting in a total amount of reconstructed $\mathit{\Lambda}$ hyperons ranging from 36k to 191k. The full reconstruction chain with all corresponding efficiency corrections was applied for each of the cut variations. All systematic errors are based on these cut variations and represent the maximum/minimum deviation to the results obtained with the chosen cut values in Table 1.

Figure 2 shows the invariant-mass spectrum of all proton-π^- pairs which passed the cuts listed in Table 1. An event-mixing technique has been used to model the combinatorial background of uncorrelated pairs. Displayed in Fig. 2 as a grey shaded histogram, the mixed event background was normalized to the data on the left and right side of the $\mathit{\Lambda}$ peak. In total, for the optimal cut selection listed in Table 1, about 100000 $\mathit{\Lambda}$ hyperons were reconstructed, with a mean signal-to-background ratio of 0.56. From a Gaussian fit to the peak, the pole mass is determined to be 1114.3 MeV/c^2, i.e. about 1.4 MeV/c^2 away from its listed value [19]. We attribute this small difference to residual deficiencies of our track reconstruction and detector alignment.

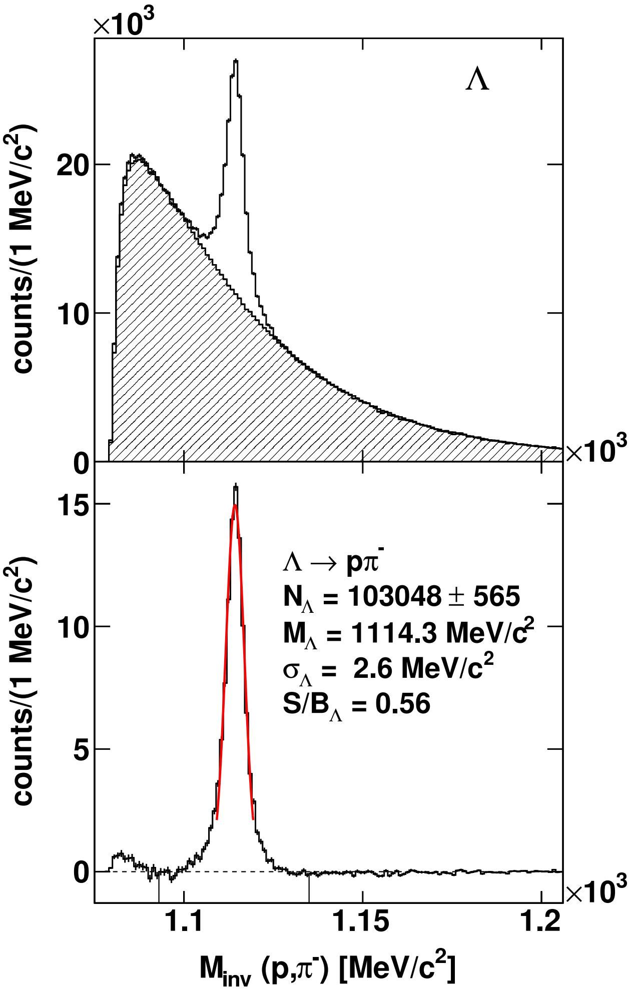

Fig. 2. Top: Invariant mass of all identified proton and π^- pairs after several cuts on the topology of the $\mathit{\Lambda}$ decay kinematics were applied (see text for details). The grey shaded histogram shows the mixed-event combinatorial background, normalized to the signal spectrum between 1080-1100 and 1130-1150 MeV/c^2. Bottom: $\mathit{\Lambda}$ signal after background subtraction; the solid red line shows a Gaussian fit to the signal.

3.2 $\mathit{\Lambda}$ spectra

For further kinematical studies the $\mathit{\Lambda}$ signal has been determined in nine rapidity bins, ranging from $-0.75 < y_{c.m.} < +0.15$ in steps of 0.1, and up to ten transverse mass bins in steps of 50 MeV/c^2. The background subtracted signal yields were corrected for acceptance and reconstruction efficiency using a full GEANT simulation of the detector system described in [14] and a track-embedding method. The geometrical acceptance, which also includes the branching ratio of $\mathit{\Lambda} \rightarrow p + \pi^-$ of 0.639, shows a smooth behaviour as a function of the transverse mass and varies for most of the bins between 13% and 34%. It is defined by the requirement that both daughter particles have hits in all MDC planes. The $\mathit{\Lambda}$ reconstruction efficiency is composed of the single track reconstruction and particle identification efficiencies (≈80% per track) and the cuts on the $\mathit{\Lambda}$-hyperon decay topology. The latter one clearly dominates the reconstruction efficiency which has values of 3% to 10%. The dominant topology cut is the one applied on the distance between the primary vertex and the $\mathit{\Lambda}$-decay vertex. It is in the order of the $\mathit{\Lambda}$-hyperon mean decay length (see Table 1). Acceptance and reconstruction efficiency are plotted for the mid-rapidity region in Fig. 3.

The acceptance- and efficiency-corrected transverse-mass spectra of $\mathit{\Lambda}$ for the various rapidity bins are presented in Fig. 4. Shown is the number of counts per LVL1

Table 1. Topological conditions values chosen for the Λ analysis (see text).

Cut	d$_{V0}$	d$_p$	d$_{\pi^-}$	d$_{dca}$	d$_{p\pi^-}$	$\alpha_{p\pi^-}$
Value	>70mm	>4.0mm	>d$_p$	<10mm	<10mm	>14°

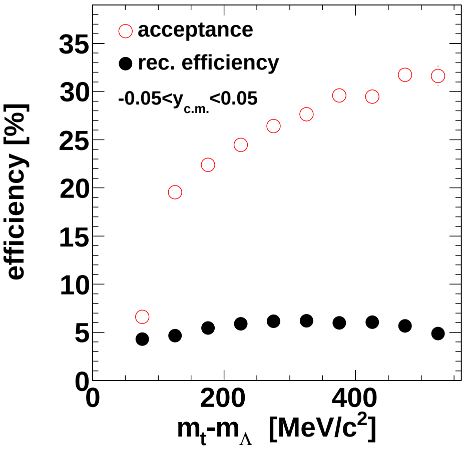

Fig. 3. (Color online) Acceptance and reconstruction efficiency at mid-rapidity for Λ-hyperons as a function of the reduced mass. The plotted acceptance (red open circles) includes already the branching ratio of 0.639 of $\Lambda \to p + \pi^-$. The reconstruction efficiency (black filled circles) consists of the single track reconstruction efficiencies of the daughter particles and the efficiencies of the topological cuts applied to improve the signal-to-background ratio (see text for details).

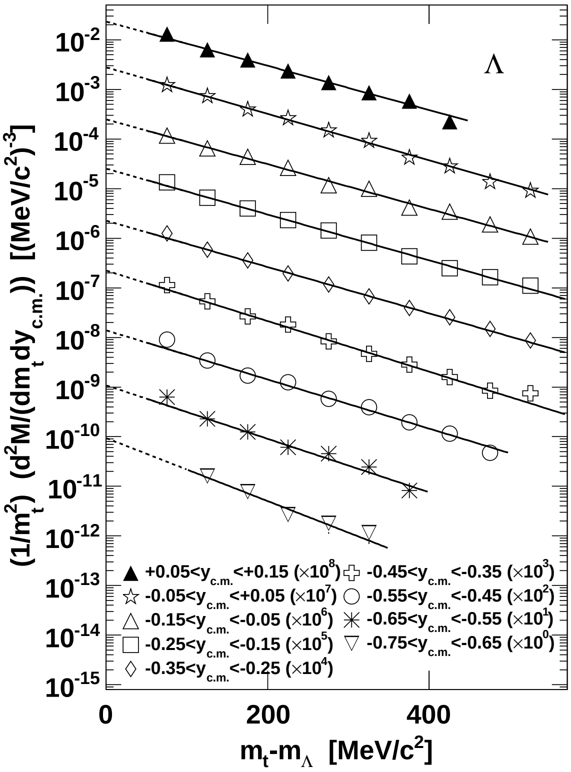

Fig. 4. Reduced $(m_t - m_\Lambda)$ transverse mass spectra for different rapidity selections. For better legibility, the spectra are scaled as indicated in the legend. The solid lines are fits with Eq. 1 to the data.

trigger, per transverse mass and per rapidity bin, divided by m_t^2. This representation is chosen in order to easily apply Boltzmann fits to the resulting distributions, according to

$$\frac{1}{m_t^2}\,\frac{d^2M}{dm_t dy_{c.m.}} = C(y_{c.m.})\,\exp\left(-\frac{(m_t - m_0)c^2}{T_B(y_{c.m.})}\right). \qquad (1)$$

The solid lines in Fig. 4 show the results of Boltzmann fits, where $T_B(y_{c.m.})$ represents the inverse slope of each distribution. The resulting $T_B(y_{c.m.})$ values are then plotted in Fig. 5 as a function of the center-of-mass (cm) rapidity ($y_{c.m.} = y - y(cm)$, where $y(cm) = 0.858$ for symmetric collisions at 1.76A GeV). The full symbols display the measured data, whereas the open ones are the data reflected at c.m. rapidity. The error bars represent the statistical errors. Assuming a thermal source, these temperatures are expected to follow the relation

$$T_B(y_{c.m.}) = \frac{T_{eff}}{\cosh(y_{c.m.})}, \qquad (2)$$

yielding an effective temperature of $T_{eff} = (95.5 \pm 0.7(\text{stat.}) + 2.2(\text{syst.}))$ MeV. Here the systematic error corresponds to the variation of the cut values described above.

For each rapidity bin the transverse mass spectrum was integrated in the following way: the yields in the covered bins were added and the fits were used to extrapolate into the unmeasured kinematic regions. The fits were integrated from 0 to the lower bin edge of the first measured point and from the upper bin edge of the last measured point to infinity. The fraction of the extrapolated yield in the transverse mass spectra to the total yield is 36-43% for the rapidity bins in the range $-0.65 < y_{c.m.} < 0.15$, and 65% for the rapidity interval $(-0.75 < y_{c.m.} < -0.65)$. The results are shown in Fig. 6, where the obtained rapidity density distribution is displayed. The full triangles show the values calculated by the integration of the transverse mass spectra, while the open triangles represent points reflected with respect to the center-of-mass rapidity.

For the determination of the total Λ multiplicity per LVL1 event, the measured spectra were integrated. The extrapolation into the unmeasured region was done by fitting either a gaussian or a linear function to the first four data points, as shown in Fig. 6. The mean value of these two different extrapolations is used for the total yield.

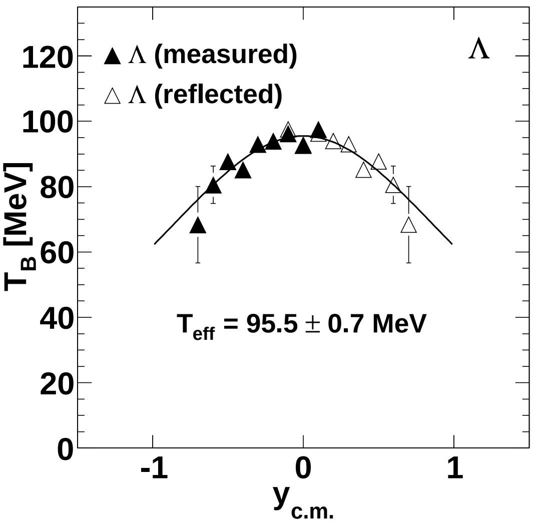

Fig. 5. Inverse-slope parameters from fits with Eq. (1) to the Λ hyperon transverse mass spectra as a function of rapidity. The solid line is a fit with Eq. (2) to the data points. The effective temperature T_{eff} is the function value at mid rapidity.

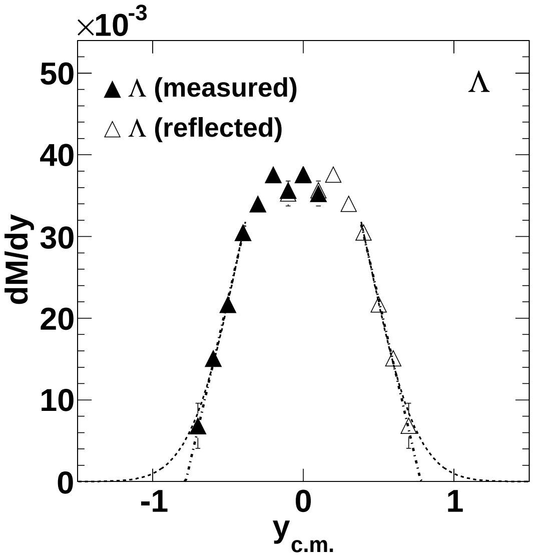

Fig. 6. Rapidity distribution of Λ hyperons. The closed symbols refer to measured data points calculated from the transverse mass spectra, whereas the open symbols show the data points reflected about center-of-mass rapidity. For the extrapolation to unmeasured rapidity values a linear and a Gaussian function were fitted to the first four data points (see text).

The fraction of the Gaussian extrapolation to the total yield is about 4.2%, whereas the fraction of the linear extrapolation is negligible. The inclusive total Λ multiplicity per LVL1 event was found to be $(4.09 \pm 0.1(\text{stat.}) \pm 0.17(\text{extr.})^{+0.17}_{-0.37}(\text{syst.}))\times 10^{-2}$, where the second error refers to the extrapolation uncertainty in m_t and the third one to the systematic error obtained from the cut variations. A detailed description of the Λ analysis can be found in [20].

4 Discussion

4.1 Particle yields

Knowing the yield of the Λ+Σ^0 hyperons and the $\Xi^-/(\Lambda+\Sigma^0)$ ratio yields the production rate of the Ξ^- to $(2.3 \pm 0.9)\times 10^{-4}$, adding statistical and systematic errors quadratically. Note that this value is of the same order of magnitude as the yield of the ϕ meson [11].

Table 2 summarizes all particle yields extrapolated to full phase space as well as the corresponding inverse slope parameters from fits to the particle m_t spectra; results on K^+, K^-, K^0_s, and ϕ are taken from [11,14].

4.2 Strangeness balance

The strong interaction conserves strangeness, i.e. the numbers of s and $\bar{s}$ quarks produced in a heavy ion reaction must be equal. As those quarks are ultimately bound in hadrons the multiplicities of strange particles fulfill a balance equation which can be written at SIS energies as:

$$K^+ + K^0 = \Sigma^{0\pm} + \Lambda + K^- + \bar{K^0} + 2\Xi^{0,-} \qquad (3)$$

where, for simplicity, the symbols denoting the particles stand for their respective yields at the time of production. Note that this equation takes care of the strong decay of heavier strange resonances via the counting of their decay products, namely kaons and Λs. As mentioned earlier, the Σ^0 can not be separated from the Λ, thus this contribution is to be counted explicitly together with Λs. Analogously, according to our analysis procedure, most $\Xi^{-,0}$ decay products feed the Λ channel and are counted as Λs, therefore the factor in Eq. (3) in front of the $\Xi^{-,0}$ is two instead of four. (Note that anyhow the $\Xi^{-,0}$ contributions are small.) In case of the neutral kaons, we measure in fact the yield of the K^0_s, which obeys the equality $K^0_s = (K^0 + \bar{K^0})/2$. Assuming isospin symmetry the yield of the $\bar{K^0}$ should be contributing here at the same order as the K^- yield. Eq. (3) can then be rewritten using the measured yields. Hence the unobserved $\Sigma^{\pm}$ hyperon yield can be estimated as:

$$\Sigma^+ + \Sigma^- = K^+ + 2K^0_s - (\Sigma^0 + \Lambda) - 2\Xi^- - 3K^- \qquad (4)$$

Still heavier multi-strange particles, e.g. Ω hyperons, have significantly higher production thresholds and should not contribute sizeably at SIS energies. From Eq. (4) a total multiplicity of charged Σ hyperons of $(7.5 \pm 6.5) \times 10^{-3}$ is deduced when using the values of the multiplicities listed in Table 2. The error is the quadratic sum of the statistical and systematic error of the different yields. If one assumes isospin symmetry for the $\Sigma^{\pm,0}$ yields one can subtract the Σ^0 contribution from the Λ yield and finds the ratio $\Sigma^{\pm,0}/\Lambda$ is 0.3 ± 0.26 although the difference in mass is only 10%.

Table 2. Multiplicities (i.e. yield/LVL1 event) and effective temperatures of particles produced in Ar+KCl reactions at 1.76A GeV. The error on the Σ and Ξ^- yield is the quadratically added statistical and systematic error.

Particle	Multiplicity	T_{eff} [MeV]	Reference
π^-	$3.9 \pm 0.1 \pm 0.1$	$82.4 \pm 0.1^{+9.1}_{-4.6}$	[14]
$\Lambda + \Sigma^0$	$(4.09 \pm 0.1 \pm 0.17^{+0.17}_{-0.37}) \times 10^{-2}$	$95.5 \pm 0.7 + 2.2$	this work
K^+	$(2.8 \pm 0.2 \pm 0.1 \pm 0.1) \times 10^{-2}$	$89 \pm 1 \pm 2$	[11]
K^0_S	$(1.15 \pm 0.05 \pm 0.09) \times 10^{-2}$	92 ± 2	[14]
K^-	$(7.1 \pm 1.5 \pm 0.3 \pm 0.1) \times 10^{-4}$	$69 \pm 2 \pm 4$	[11]
ϕ	$(2.6 \pm 0.7 \pm 0.1 - 0.3) \times 10^{-4}$	84 ± 8	[11]
Ξ^-	$(2.3 \pm 0.9) \times 10^{-4}$	-	[15]
$\Sigma^+ + \Sigma^-$	$(0.75 \pm 0.65) \times 10^{-2}$	-	estimated via strangeness balance

The only other published multiplicity of charged Σ hyperons in heavy ion collisions, based on a similar analysis of strangeness yields measured with the FOPI detector at GSI in Ni+Ni reactions at 1.93A GeV, is $(7 \pm 8 + 32 - 17) \times 10^{-3}$ [16]. Differences with respect to our analysis are: (1) a higher beam energy (1.93 vs. 1.76A GeV), (2) a larger reaction system (58+58 vs. 40+37), and (3) a different centrality selection ($\langle A_{part} \rangle = 71$ vs. 38.5) resulting in a higher Λ yield $(0.137 \pm 0.005 + 0.007 - 0.008)$ and inverse slope parameter $(119 \pm 1 + 9 - 7)$. In view of the higher bombarding energy and larger system size, one would expect a larger charged Σ contribution. The resulting $\Sigma^{\pm,0}/\Lambda$ ratio is $0.08 \pm 0.09 + 0.33 - 0.18$. Unfortunately, the large uncertainties prevent us to draw a firm conclusion on the behavior of the respective cross sections with energy.

4.3 Comparison with statistical hadronization

Statistical hadronization models (SHM) have been successful in fitting particle yields or yield ratios from relativistic and ultrarelativistic heavy ion collisions [21,22, 23,24]. With the help of SHM fits it has been possible to reconstruct systematically the chemical freeze-out line in the T − μ_b plane of the nuclear phase diagram with μ_b being the baryochemical potential (see e.g. [24,26]). However, while the various SHM approaches agree fairly well at high bombarding energies, discrepancies appear in the low-energy regime. Indeed, at the lower energies it is not even clear, whether chemical equilibrium can be reached [27] and therefore the question arises whether a statistical treatment of particle production is meaningful. The situation is further complicated by the need for strangeness suppression, which is handled differently in the various SHM implementations. Furthermore, at SIS energies, only pions are produced abundantly. Heavier and especially strange particles are rare, and their yields were mostly poorly known. Hence in the past only few particle yields with small statistical errors were available as input to the fit procedure. In the following we fit eight particle yields obtained from our Ar+KCl run with a statistical hadronization model.

We choose the freely available THERMUS code [28], using the mixed canonical ensemble where strangeness is exactly conserved while all other quantum numbers are calculated grand canonically. We handle the strangeness suppression by introducing a strangeness correlation radius R_c within which strangeness has to be exactly conserved; this is discussed in [29]. We fit simultaneously all particle yields listed in Table 2 except for the $\Sigma^{\pm}$, as well as the mean number of participants $\langle A_{part} \rangle$ and constrain the charge chemical potential μ_Q using the ratio of the baryon and charge numbers of the collision system. We find the chemical freeze-out at a temperature of $T_{chem} = (76 \pm 2)$ MeV and at a baryochemical potential of $\mu_b = (799 \pm 22)$ MeV. The strangeness correlation radius comes out as $R_c = (2.2 \pm 0.2)$ fm, which corresponds to about half the fitted radius $R = (4.1 \pm 0.5)$ fm of the whole fireball. The exclusion of the Ξ^- from the fit changes the parameters only on the percent level, but the χ^2/d.o.f. value of the fit improves from 13.9/4 to 7.8/3. Fig. 7 shows the resulting freeze-out point together with a compilation of similar points [30,24,31] in the T − μ_b plane. Our result, as well as the FOPI result from the collision system Al+Al at 1.9A GeV, differ from the regularity of freeze-out points following the fixed energy per particle condition $\langle E \rangle / \langle N \rangle \approx 1$ GeV, which is one of the commonly proposed freeze-out criteria [24]. This might be due to the light collision systems, since small systems have the tendency to show higher freeze-out temperatures [25].

A detailed comparison of the data with the statistical model fit is shown in the upper part of Fig. 8, while the lower part of this figure depicts the ratio of data and fit. All particles except for the Ξ^- are well described.

A particularly interesting case is the ϕ meson. The ϕ is treated as a strangeness neutral object in the R_c formalism and is therefore not suppressed at all. Its yield is well described by the SHM. This means that the ϕ yield is compatible with the assumption that it takes part in the equilibration of the hadrons. This is quite different from the situation at higher bombarding energies, where the ϕ requires indeed an effective strangeness between 1 and 2 to have the appropriate suppression in the SHM and to reproduce the data [29]. For an understanding of ϕ production, one may have a look at the ϕ/K^- ratio which, according to the SHM with R_c, should rise at low beam energy. Such a behavior is indeed supported by our data,

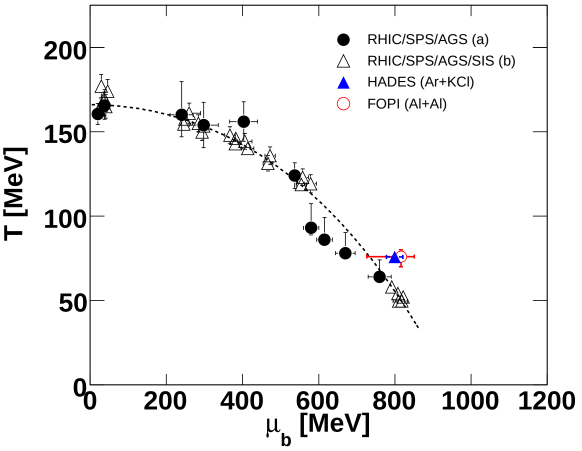

Fig. 7. (Color online) Chemical freeze-out points in the T – μ_b plane. The filled black circles (a) are taken from [30], the black open triangles (b) are from [24]. The red circle is taken from [31]. The THERMUS fit to our Ar+KCl data is shown as blue triangle. The dashed line correponds to a fixed energy per nucleon of 1 GeV, calculated according to [24].

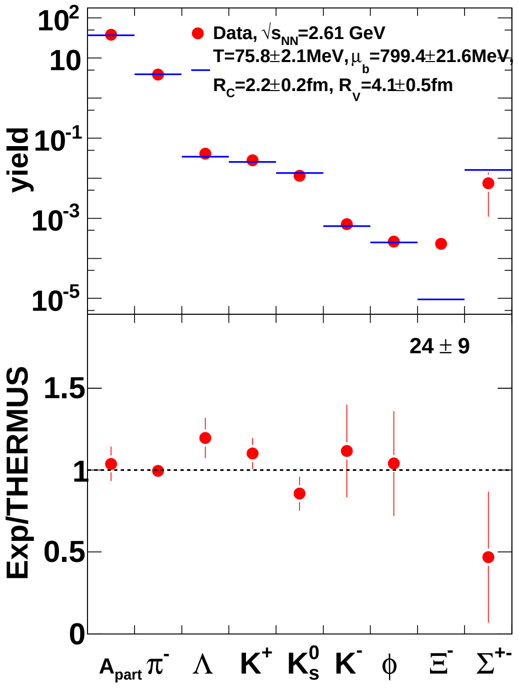

Fig. 8. (Color online) The upper plot shows the yields of secondary hadrons in Ar+KCl reactions (filled red circles) and the corresponding THERMUS fit (blue bars). The lower plot shows the ratio of the experimental value and the SHM value. For the Ξ^- the ratio number is quoted instead of a point.

as already discussed in [11], and the ratio seems to approach the value seen in elementary NN reactions [32].

According to the strangeness suppression mechanism implemented in SHM, the double-strange Ξ^- (S=2) should be suppressed strongly with respect to the ϕ with its hidden strangeness (S=0). Nevertheless, our measured Ξ^- yield is of the same magnitude as the one of the ϕ, i.e. the data show no indication for any strangeness suppression. This is very surprising since the Ξ^- yields observed above threshold at RHIC [33], at SPS [34] and even at AGS [35] are consistent with statistical model fits. In fact the same secondary pion-hyperon process $\pi + Y \to \phi + Y$, which was invoked by Kolomeitsev and Tomasik [36] to explain the enhanced ϕ yield, can here be the origin of the high Ξ production via the reaction $\pi + Y \to \Xi + K$. To get a better understanding, we may have to move away from the SHM. One may calculate the probability for the production of two $s\bar{s}$ pairs in one collision. Assuming that both pairs are independently created, their production probability $P_{2s\bar{s}}$ is given as the square of the single-pair production probability $P_{s\bar{s}}$. Keeping associated production in mind, $P_{s\bar{s}}$ can be estimated as the combined multiplicity of all particles that carry a strange quark, respectively the combined multiplicity of all anti-strange particles, i.e. $K^+ + K^0 + \phi$, yielding $P_{s\bar{s}} \simeq 0.05$ and hence $P_{2s\bar{s}} \simeq 0.0025$. Considering that the observed Ξ^- yield is in fact an order of magnitude smaller, we conclude that in 10% of these events both s quarks end up together in a Ξ^-, whereas from strangeness suppression in the SHM one obtains less than 1%. A different realization of the SHM using the strangeness canonical ensemble and γ_s for additional strangeness suppression delivers comparable freeze-out parameters, with $T_{chem} = (76 \pm 5)$ MeV, $\mu_b = (791 \pm 33)$ MeV, $R = (4.1 \pm 0.9)$ fm and $\gamma_s = 0.37 \pm 0.04$ but fails to reproduce the ϕ multiplicity by an order of magnitude due to its suppression with γ_s^2.

4.4 Chemical vs. kinetic freeze-out

The temperature T_{chem} obtained for the chemical freeze-out can be compared with the inverse-slope parameter T_{eff} obtained from Boltzmann fits to the m_t spectra of the different particle species. Apparently most of the inverse-slope parameters are higher than the chemical freeze-out temperature of the system. A pure Boltzmann shape can be distorted by various effects, like collective motion or early vs. late particle decays. One example is apparent in the difference between the K^+/K^0_s and K^- slopes (see Fig. 9). The much lower value of T_{eff} of the K^- has often been interpreted as due to its much later freeze-out time [12] neglecting the admixture of soft K^- stemming from ϕ decays. In [37] however it was shown that these soft K^- indeed affect the shape of the spectra.

Effects of collective flow, on the other hand, should influence the transverse mass slope more, the higher the particle mass. From Fig. 9, where the fitted temperatures are ordered by increasing particle mass, this seems not to be a strong effect as expected for a small collision system

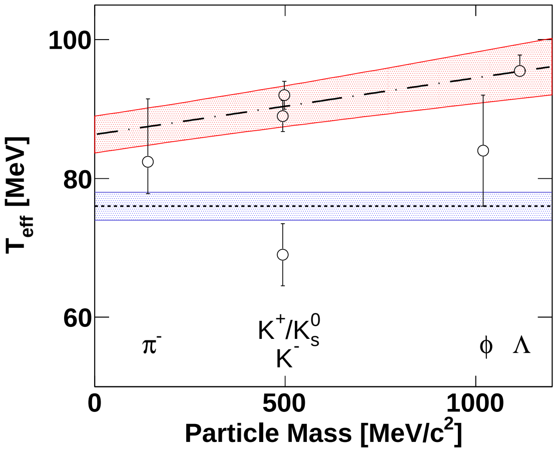

Fig. 9. (Color online) Effective temperature T_{eff} of all measured particle species as a function of their mass. The horizontal line and error band show the chemical freeze-out temperature T_{chem} from the THERMUS fit, whereas the dashed-dotted line and the red error band show a linear fit to the data points (K^- are excluded, see text for details).

like Ar+KCl. However the inverse-slope parameter seems to be slightly decreasing with decreasing mass.

To take this effect into account a linear fit to the data points was applied (dashed-dotted line and red error band in Fig. 9). The K^- were excluded from the fit for the reasons discussed above. The fit is clearly dominated by the Λ and K^+/K^0_s data points with small relative errors compared to the ϕ and π^- data points. Within errors, the extrapolated fit value at mass 0 is still above the chemical freeze-out temperature. Hence the presented data implies an inversion of the kinetic- and chemical freeze-out scenario, which cannot be the case for obvious reasons. This means either the statistical model approach for small reaction systems and small energies is not applicable, and/or the unique kinetic freeze-out for all particles with one radial flow velocity is a too naive assumption for this system. Future measurements of HADES in the reaction systems Au+Au and Ag+Ag will give more insight into the complex dynamics at low energies.

5 Summary and conclusions

We have presented phase space distributions of Λ hyperons in Ar+KCl at 1.76A GeV measured with the HADES spectrometer at GSI. Combining the measured $\Lambda + \Sigma^0$ yield with our former data on strangeness production in this system we have estimated the yield of the double-strange Ξ^- hyperon. We find that it is of the same order of magnitude as the one of the ϕ meson. The fraction of the unobserved charged $\Sigma^\pm$ hyperons could be constructed using strangeness conservation.

Applying a statistical model fit to these hadron yields, a fair agreement, except for the Ξ^-, in a strangeness-canonical approach is achieved. The ϕ, however, is well reproduced without any suppression, in sharp contrast to the situation at higher energies, where a suppression is observed.

The HADES collaboration gratefully acknowledges the support by BMBF grant 06MT9156, 06GI146I,06FY171 and 06DR9059D (Germany), by GSI (TMKrue 1012, GI /ME3, OF/STR), by Excellence Cluster Universe (Germany), by grants GA AS CR IAA100480803 and MSMT LC 07050 MSMT (Czech Republic), by grant KBN5P03B 140 20 (Poland), by INFN (Italy), by CNRS/IN2P3 (France), by grants MCYT FPA2000-2041-C02-02 and XUGA PGID FPA2009-12931 T02PXIC20605PN (Spain), by grant UCY-10.3.11.12 (Cyprus), by INTAS grant 06-1000012-8861 and EU contract RII3-CT-506078.

References

1. C. Sturm *et al.* (KaoS Collaboration), Phys. Rev. Lett. **86**, 39 (2001).
2. C. Fuchs, A. Faessler, E. Zabrodin, Phys. Rev. Lett. **86**, 1974 (2001).
3. C. Hartnack, J. Aichelin, J. Phys. G **28**, 1649 (2002).
4. C. Hartnack, H. Oeschler and J. Aichelin, Phys. Rev. Lett. **96**, 012302 (2006).
5. J. Schaffner-Bielich, J. Bondorf, A. Mishustin, Nucl. Phys. A **625**, 325 (1997).
6. W. Cassing, E. L. Bratkovskaya, U. Mosel, S. Teis, A. Sibirtsev, Nucl . Phys. A **614** 415 (1997).
7. F. Uhlig *et al.* (KaoS Collaboration), Phys. Rev. Lett. **95**, 12301 (2005).
8. C. Hartnack, H. Oeschler and J. Aichelin, Phys. Rev. Lett. **90**, 102302 (2003).
9. A. Förster *et al.* (KaoS Collaboration), Phys. Rev. Lett. **91**, 152301 (2003).
10. H. Schade, Gy. Wolf and B. Kämpfer, Phys. Rev. C **81**, 034902 (2010).
11. G. Agakishiev *et al.* (HADES Collaboration), Phys. Rev. C **80**, 025209 (2009).
12. A. Förster *et al.* (KaoS Collaboration), Phys. Rev. C 75, 024906 (2007).
13. C. Fuchs, Progr. Part. Nucl. Phys. **56**, 1 (2006).
14. G. Agakishiev *et al.* (HADES Collaboration), Phys. Rev. C 82, 044907 (2010).
15. G. Agakishiev *et al.* (HADES Collaboration), Phys. Rev. Lett. **103**, 132301 (2009).
16. M. Merschmeyer *et al.* (FOPI Collaboration), Phys. Rev. C **76**, 024906 (2007).
17. G. Agakishiev *et al.* (HADES Collaboration), Eur. Phys. J. A **41**, 243 (2009).
18. S. A. Bass *et al.*, Prog. Part. Nucl. Phys. **41** 225 (1998).
19. C. Amsler *et al.* (Particle Data Group), Phys. Lett. B **667**, 1 (2008).
20. A. Schmah, PhD thesis, Technical University Darmstadt, Darmstadt (2008).
21. R. Averbeck, R. Holzmann, V. Metag and R. S. Simon, Phys. Rev. C **67**, 024903 (2003).
22. F. Becattini, M. Gazdzicki, A. Keranen, J. Manninen and R. Stock, Phys. Rev. C **69**, 024905 (2004).
23. P. Braun-Munzinger, K. Redlich and J. Stachel, arXiv:nucl-th/0304013 (2003).
24. J. Cleymans, H. Oeschler, K. Redlich and S. Wheaton, Phys. Rev. C **73**, 034905 (2006).

25. J. Cleymans *et al.*, Phys. Rev. C 59, 1663 (1999).
26. A. Andronic *et al.*, Nucl. Phys. A **837** 65 (2010).
27. V. Koch, J. Phys. G **30**, S41 (2004).
28. S. Wheaton and J. Cleymans, Comput. Phys. Commun. **180**, 84 (2009).
29. I. Kraus, J. Cleymans, H. Oeschler, K. Redlich and S. Wheaton, Phys. Rev. C **76**, 064903 (2007).
30. A. Andronic, P. Braun-Munzinger and J. Stachel, Nucl. Phys. A **772**, 167 (2006).
31. X. Lopez *et al.* (FOPI Collaboration), Phys. Rev. C **76**, 052203 (2007).
32. Y. Maeda *et al.* (ANKE Collaboration), Phys. Rev. C **77**, 015204 (2008).
33. J. Adams *et al.* (STAR Collaboration), Phys. Rev. Lett. **98**, 062301 (2007).
34. F. Antinori *et al.* (NA57 Collaboration), Phys. Lett. B **595**, 68 (2004).
35. P. Chung *et al.* (E895 Collaboration), Phys. Rev. Lett. **91**, 202301 (2003).
36. E. E. Kolomeitsev and B. Tomasik, J. Phys. G **36**, 095104 (2009).
37. M. Lorenz *et al.* (HADES Collaboration), PoS BORMIO2010 (2010) 038.